12-20-2013

Promoting Electrocatalytic Activity of a Composite SOFC Cathode $La_{0.8}Sr_{0.2}MnO_{3+\delta}/Ce_{0.8}Gd_{0.2}O_{2-\delta}$ with Molten Carbonates

Yunhui Gong

Xue Li

Lingling Zhang

Whitney Tharp

Changyong Qin

See next page for additional authors

Publication Info

Published in *Journal of The Electrochemical Societye*, Volume 161, Issue 3, 2013, pages F226-F232.
©Journal of The Electrochemical Society 2013, The Electrochemcial Society.

Publisher's Version: *http://dx.doi.org/10.1149/2.034403jes*

Gong, Y., Li, X., Zhang, L., Tharp, W., Qin, C., & Huang, K. (December 20, 2013). Promoting Electrocatalytic Activity of a Composite SOFC Cathode $La_{0.8}Sr_{0.2}MnO_{3+\delta}/Ce_{0.8}Gd_{0.2}O_{2-\delta}$ with Molten Carbonates. Journal of The Electrochemical Society, 161 (3), F226 – F232. http://dx.doi.org/10.1149/2.034403jes

Journal of The Electrochemical Society, **161** (3) F226-F232 (2014)
0013-4651/2014/161(3)/F226/7/$31.00 © The Electrochemical Society

Promoting Electrocatalytic Activity of a Composite SOFC Cathode $La_{0.8}Sr_{0.2}MnO_{3+\delta}/Ce_{0.8}Gd_{0.2}O_{2-\delta}$ with Molten Carbonates

Yunhui Gong,[a] Xue Li,[a] Lingling Zhang,[a] Whitney Tharp,[a] Changyong Qin,[b] and Kevin Huang[a,*,z]

[a]*Department of Mechanical Engineering, University of South Carolina, Columbia, South Carolina 29201, USA*
[b]*Department of Biology, Chemistry and Environmental Health Science, Benedict College, Columbia, South Carolina 29204, USA*

The effect of molten carbonates (MCs) on polarization resistance (R_P), a direct measure of oxygen reduction reaction (ORR) activity, of a composite $La_{0.8}Sr_{0.2}MnO_{3+\delta}/Ce_{0.8}Gd_{0.2}O_{2-\delta}$ (LSM/GDC) solid oxide fuel cell (SOFC) cathode has been systematically investigated in this study over a temperature range of 550–650°C and partial pressure of oxygen (pO_2) span of $10^{-3} \sim 1$ atm. It is shown that the LSM/GDC cathode, either in the pristine or MC-modified states, can be generally modeled by two consecutive parallel circuits consisting of a resistance and a constant phase element (CPE). The high-frequency $R_{P(HF)}$//$CPE_{(HF)}$ component is related to a charge-transfer process, while the low-frequency $R_{P(LF)}$//$CPE_{(LF)}$ counterpart is associated with a surface oxygen dissociative adsorption process. Incorporation of an adequate amount of MC significantly reduces $R_{P(LF)}$ by as much as a factor of 10. Studies on the dependence of R_P on temperature and pO_2 further reveal that the rate-limiting step of a LSM/GDC cathode has shifted from the original surface oxygen dissociative adsorption to the formation of an intermediate CO_4^{2-} species in the presence of MC.
 [DOI: 10.1149/2.034403jes]

Manuscript submitted November 14, 2013; revised manuscript received December 11, 2013. Published December 20, 2013.

The Sr-doped $LaMnO_3$ (LSM) is one of the most promising cathode materials for solid oxide fuel cells (SOFCs) because of its high electronic conductivity and excellent thermal/chemical compatibility with ZrO_2-based electrolytes.[1–3] However, it has to operate above 800°C where LSM maintains a good electrocatalytic activity to the oxygen reduction reaction (ORR). At reduced temperatures, LSM quickly loses its ORR activity because of the lack of ionic conductivity, becoming a poor electrocatalyst with high polarization resistance (R_P) for ORR. Many attempts have been made in the past to render it useable for reduced temperature SOFCs. Most efforts are noted in the areas of 1) forming composite with electrolytes;[4,5] 2) roughening the cathode/electrolyte interface;[6,7] 3) optimizing manufacturing conditions;[8] 4) infiltrating active nanoscaled catalysts.[9,10] Overall, a common goal of these approaches is to promote ORR activity through the mechanisms of increasing LSM's mixed ionic-electronic conductivity and reactive surface areas.

Parallel to these efforts, we have recently demonstrated a different philosophy to achieve the same goal: use of molten carbonates (MCs) as an unconventional ORR electrocatalyst.[11,12] The rationale of this approach is primarily based on early studies that showed molten carbonates possessing good catalytic activity to reduce O_2 molecules in molten carbonate fuel cells (MCFCs).[13–15] Different from the conventional ORR mechanisms perceived for SOFC composite cathodes, the ORR pathways in the presence of MCs have also been proposed to follow the consecutive steps of:[11,12]

1) Formation of CO_5^{2-} and CO_4^{2-} at the O_2/MC surface:

$$CO_3^{2-}{}_{MC} + O_{2_{air}} \rightarrow CO_5^{2-}{}_{MC} \quad [1]$$

$$CO_5^{2-}{}_{(MC)} + CO_3^{2-}{}_{(MC)} \rightarrow 2CO_4^{2-}{}_{(MC)} \quad [2]$$

2) Migration of CO_4^{2-} species towards the MC/cathode interface, where CO_4^{2-} species are further reduced by the electrons from cathode into O^{2-} in the cathode and CO_3^{2-} in the MC phase:

$$CO_4^{2-}{}_{(MC)} + 2e^-{}_{(LSM)} \rightarrow CO_3^{2-}{}_{(MC)} + O^{2-}{}_{(LSM-GDC-MC)} \quad [3]$$

The migration of oxygen in CO_4^{2-} follows a cooperative "cogwheel" mechanism, which is similar to the superionic conduction observed in fast alkali-metal ionic conductors.[16–18]

3) The produced $O^{2-}{}_{(LSM-GDC-MC)}$ continues to migrate across the cathode/electrolyte interface, while $CO_3^{2-}{}_{(MC)}$ migrates back toward the O_2/MC surface to replenish the MC phase.

The existences of CO_4^{2-} and CO_5^{2-} intermediate species are supported by both DFT calculations[11] and in-situ Raman spectroscopy.[19]

The aim of this study is to provide electrochemical evidence for the above charge-transfer model by investigating the dependence of R_P of a MC-modified $La_{0.8}Sr_{0.2}MnO_{3+\delta}/Ce_{0.8}Gd_{0.2}O_{2-\delta}$ (LSM/GDC) cathode on temperature (T) and partial pressure of oxygen (pO_2), from which the rate-limiting steps and charge-transfer mechanisms can be better understood. Since the ORR for LSM/GDC is limited by the surface oxygen exchange,[20,21] the effect of MC on the surface oxygen exchange kinetics occurring in the LSM/GDC cathode can be best exploited.

Experimental

Fabrication of LSM/GDC symmetrical cells.— Symmetrical cell configuration, consisting of two identical thin porous LSM/GDC cathode layers separated by a dense 250-μm thick LSGM ($La_{0.8}Sr_{0.2}Ga_{0.83}Mg_{0.17}O_{3-\delta}$) electrolyte membrane, was used to investigate the electrochemical polarization resistance. The LSGM electrolyte membrane was fabricated by a standard tape casting method described in ref 22. Fine LSGM powders were made through a solid state reaction and ball milling,[23] followed by full dispersing and mixing them in solvent (Terpineol, Aldrich) with addition of dispersant (Hypermer, Croda), Binder (Ethyl cellulose, Acros) and plasticizer (Dioctyl phthalate, Acros). The homogeneous slurry was degased under vacuum and casted onto a silicone-coated Mylar film driven by a commercial tape casting machine (TTC-1200, Richard E, Mistler, Inc.). After solvent evaporation at 80°C for 12h, circular samples were cut, thermally laminated and finally fired at 1450°C for 5h. The resultant electrolyte membranes were approximately 15 mm in diameter and 250 μm in thickness.

LSM/GDC composite cathode powder was prepared from a commercial LSM and GDC powder (Fuel Cell Materials). The two powders in a weight ratio of 50/50 were first mixed and ball milled in alcohol for 24h. After drying in the oven for 12h, the composite powders were then mixed with an organic binder (V-006, Heraeus) to form the cathode ink, which was then screen printed on both sides of a tape-casted LSGM electrolyte membrane. The three-layer symmetrical structure was then calcined at 1100°C for 2h to achieve good bonding and porosity. The estimated porosity from weight loss is roughly 25%. The final symmetrical cell had an effective surface area

*Electrochemical Society Active Member.
zE-mail: kevin.huang@sc.edu

of 0.75 cm^2 and a porous cathode thickness of 20 μm. Silver paste (C8829, Heraeus) and silver meshes were used for current collectors.

Dispersion of Li/Na/K molten carbonate into LSM/GDC cathode.— The Li-Na-K carbonate was prepared by mixing lithium carbonate (99%, Alfa Aesar), sodium carbonate (99%, Alfa Aesar) and potassium carbonate (99%, Alfa Aesar) in the eutectic composition (Li/Na/K = 43.5/31.5/25.0 mol%) and melting at 600°C for 1h. The melted carbonate was ball milled into fine powders, which were then dissolved in deionized water into a precursor solution (1 g/100 mL) for infiltration. A controlled amount of carbonate was infiltrated into the porous cathode structure with the precursor solution under a vacuum condition. After each infiltration, samples were dried at 100°C in air for 12h. The carbonate loading was controlled by the number of infiltration-drying process.

Impedance and microstructural characterizations.— Electrochemical impedance spectroscopy (EIS) was carried out on the symmetrical cells with a Solartron 1260 frequency response analyzer coupled with a Solartron 1287 electrochemical interface and controlled with ZPlot software. The impedance data were collected at open circuits in the frequency range 10 mHz–100 kHz with 20 mV of stimulus AC amplitude. Measurements were taken as a function of carbonate loading (0–1.8 $mg \cdot cm^{-2}$), temperature (500–650°C) and oxygen partial pressure (0.001–1 atm). The EIS data were further analyzed to determine R_P with ZView software in conjunction of a set of equivalent electrical circuit simulations.

A commercial anode supported fuel cell (Fuel Cell Materials) consisted of a Ni-YSZ composite anode (220 μm thick), YSZ electrolyte (10 μm thick), and LSM/GDC composite cathode (50 μm thick) with or without MC-modification prepared in this study. The fuel cell performance including V-I curve and EIS was characterized with hydrogen (3%H_2O) at 50 sccm as the fuel and air at 100 sccm as the oxidant.

The microstructures of the original and MC-modified LSM/GDC composite cathodes, either in pre-tested or post-tested state, were examined with a field-emission scanning electron microscopy (FESEM, Zeiss Ultra) equipped with an energy dispersive X-ray spectroscopy (EDS) analyzer.

Results and Discussion

R_P as a function of carbonate loading.— Representative EIS spectra measured at 600°C under the open-circuit condition for different loadings of carbonate are shown in Fig. 1a. From these EIS spectra, the ohmic resistance (R_O) primarily contributed from the electrolyte is determined from the high-frequency intercepts with the real axis, whereas R_p of the cathode is determined by the arc length on the real axis between the high- and low-frequency intercepts, both of which are further illustrated in the inset of Fig. 1a.

The polarization is evidently the major contributor to resistance for each cell. For the pristine sample, R_p is as high as 40 $\Omega \cdot cm^2$ at 600°C, while R_O is only 0.95 $\Omega \cdot cm^2$. For the MC-modified cathode, a drastic reduction in R_p is noted. For instance, at 600°C, R_p is a factor of ten lower than the pristine sample, i.e. 4.0 $\Omega \cdot cm^2$ at 1.2 $mg \cdot cm^{-2}$ of carbonate loading. However, no significant difference in R_O is observed between the two samples. The optimal loading was observed at 1.2 $mg \cdot cm^{-2}$, which is also true for the entire

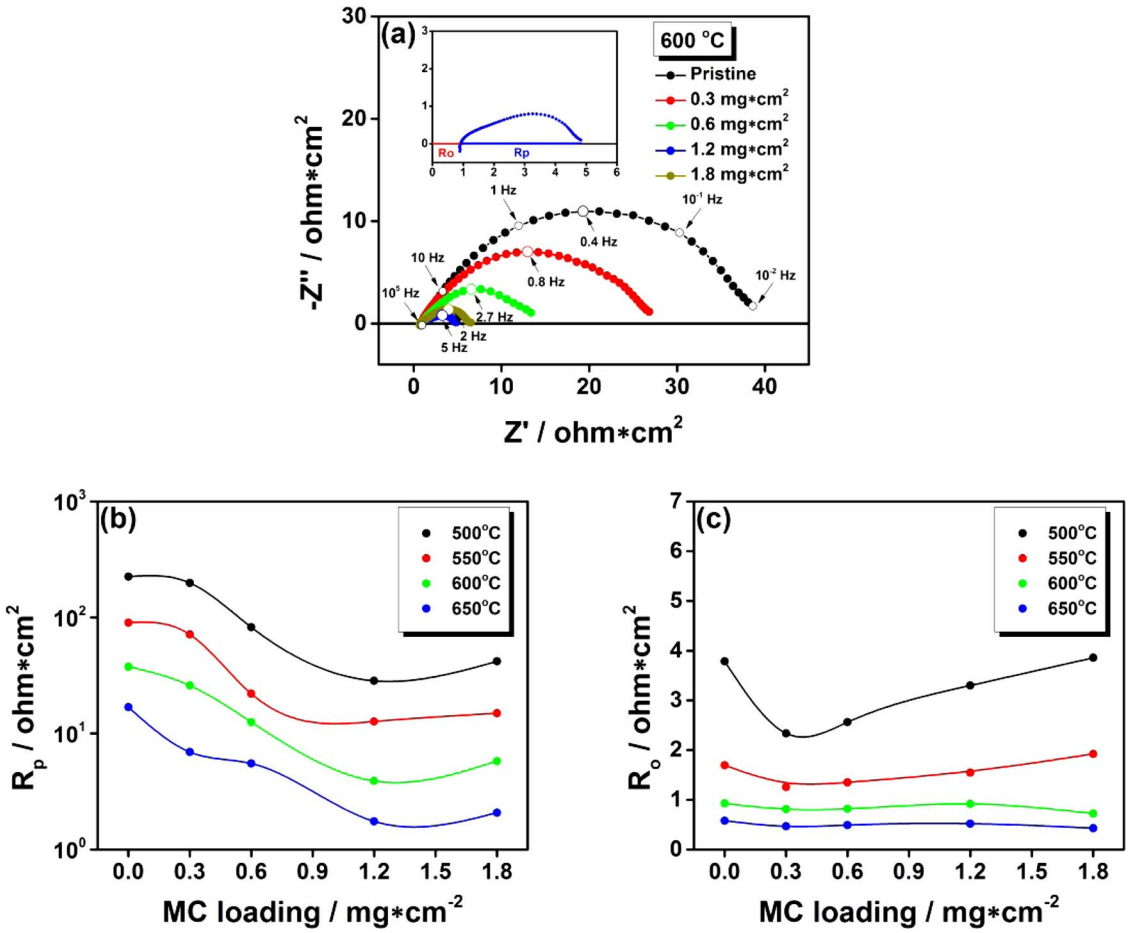

Figure 1. Dependence of R_O and R_P of an LSM/GDC cathode on MC loading: (a) EIS spectra measured at 600°C, (b) R_p and (c) R_o measured as a function of MC loading at different temperatures.

temperature range studied as shown in Fig. 1b and 1c. It is worth mentioning that the observed R_p of the pristine cathode is much greater than the values reported in the literature for similar composite cathodes, e.g., 6.81 $\Omega \cdot cm^2$ at 600°C[5] for one study and 11 $\Omega \cdot cm^2$ at 650°C for another study.[24] The variability in electrode/electrolyte composition, fabrication process and testing conditions used by different research groups is believed to contribute to the scattered data.[8,25,26] Since the nature of the present study is comparative, *i.e.* addition of MC is studied as an independent variable throughout the investigation, the conclusions drawn on the effect of MC would be applicable to other cathode compositions.

Equivalent electrical circuit simulation.— To glean insights into the ORR activity from the measured EIS spectra, further spectroscopic analysis was performed between the pristine LSM/GDC cathode and the one modified with MC at the optimal loading of 1.2 $mg \cdot cm^{-2}$. Shown in Fig. 2 are the EIS spectra measured at 600°C in Nyquist (Fig. 2a) and Bode (Fig. 2b) plots. What is observed in the Nyquist plot is a significant reduction in R_p along with a transition in shapes of the spectra observed for the MC-modified sample. The EIS spectrum of the pristine cathode seems to consist of a single depressed arc intercepting the real axis, whereas that of the MC-modified cathode is clearly shown to comprise of more than one depressed arcs. Another noticeable change is the shift in characteristic peak frequencies (f_{max}) to a higher value as marked in Fig. 2a for the MC-modified cathode.

In order to describe quantitatively the ORR processes, the EIS spectra were further analyzed by the equivalent electrical circuit model consisting of two R//CPE sub-circuits as shown in the inset of Fig. 2a. In this model, L represents the inductance arising from the measuring leads; the $R_{p(HF)}$//$CPE_{(HF)}$ and $R_{p(LF)}$//$CPE_{(LF)}$ components represent the electrode processes at high and low frequency range, respectively. The impedance of a CPE is mathematically expressed by $Z_{CPE}(j\omega) = 1/(Q^*(j\omega)^n)$, where Q is a frequency-independent real constant, ω is angular frequency, and n is exponent constant. The results of simulations are summarized in Table I. With the addition of carbonate, R_p shows a small increase in $R_{P(HF)}$ from 0.41 to 0.61 $\Omega \cdot cm^2$, but a factor of 10 reductions in $R_{P(LF)}$. The f_{max} of both the low and high frequency responses shown in Fig. 2a are notably shifted to higher end by the presence of MC. The capacitance values of CPE calculated for both samples show no significant difference and are in the order of 10^{-4} – 10^{-3} $F \cdot cm^{-2}$, which are in good agreement with these reported in previous studies.[27–29] The exponent n in $(j\omega)^n$ is found to be similar for both samples, 0.76 (pristine) vs 0.74 (MC) for the high-frequency response, but decreased from 0.68 (pristine) to 0.56 (MC) for the low-frequency response after MC modification, suggesting a less opened microstructure of the latter.[30]

Table I. Key electrochemical parameters obtained from fitting the measured EIS spectra with the equivalent electrical circuit shown in Fig. 2.

	High frequency		Low frequency	
Parameter	Pristine	MC-modified	Pristine	MC-modified
R_p ($\Omega \cdot cm^2$)	0.41	0.61	37.91	3.43
f_{max} (Hz)	71.7	891.8	0.35	5.5
$Q(\Omega^{-1} \cdot cm^{-2} \cdot sec^{-n})$	$9*10^{-3}$	$1*10^{-3}$	$5.9*10^{-3}$	$1.5*10^{-2}$
n	0.76	0.74	0.68	0.56

The Bode plots shown in Fig. 2b appear to support the frequency response over which simulations are performed and shown in the Nyquist plots. For the pristine sample, $R_{P(HF)}$ is so small compared to $R_{P(LF)}$ that it is not readily visible in the plot. This is primarily caused by the total domination by $R_{P(LF)}$ measured over a fixed frequency domain. For the MC-modified sample, separation of HF and LF processes is a little more evident due to the closeness in $R_{P(HF)}$ and $R_{P(LF)}$.

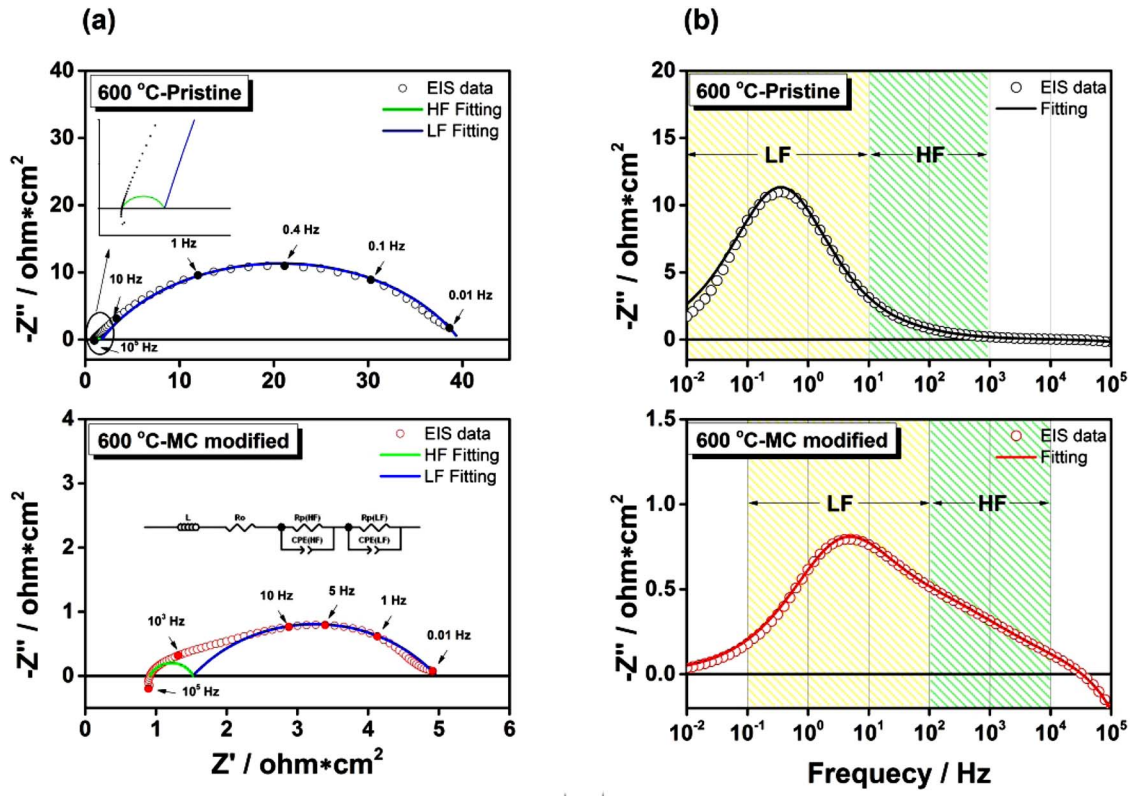

Figure 2. Comparison of EIS spectra between pristine and MC-modified LSM/GDC cathode at 600°C; (a) Nyquist plot, (b) Bode plot.

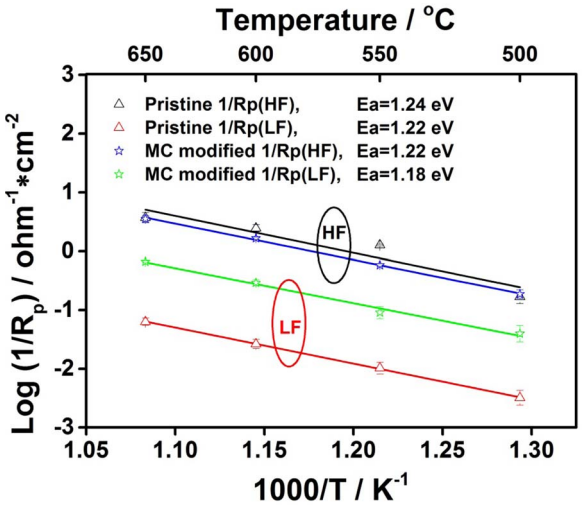

Figure 3. Arrhenius plot of high-frequency and low-frequency R_p as a function of reciprocal temperature for the pristine and carbonate modified cathodes.

The activation energy associated with each cathode process is obtained from the Arrhenius plot of $1/R_p$ as a function of 1000/T in Fig. 3. Both the low-frequency response, $R_{p(HF)}$, and the high-frequency response, $R_{p(LF)}$, obey the Arrhenius behavior. The activation energy was not affected by the presence of MC for $R_{P(HF)}$ and $R_{P(LF)}$: 1.24 eV (pristine) vs 1.22 eV (MC) for $R_{p(HF)}$ and 1.22 eV (pristine) vs 1.18 eV (MC) for $R_{P(LF)}$. These values are generally in good agreement with those reported in prior studies on LSM-based composite cathodes.[5,24,29,31,32] The pronounced difference lies in the pre-exponential factor A. In classical transport theory, A for a first-order reaction is defined as the total number of collisions (leading to a reaction or not) per second, and $e^{-Ea/(RT)}$ is the probability that any given collision would result in a reaction. For a reaction with similar activation energy, an increased number of collisions would result in an increase in the rate of a reaction. A comparison of $R_{P(LF)}$ between the pristine and MC-modified cathodes indicates pre-exponential term A a factor of ten higher for the latter than the former, implying that the presence of MC has led to an increase in the number of active species necessary for a faster ORR originally limited by the slow surface oxygen dissociative adsorption.

Effect of pO_2 on R_P.— Studying the dependence of R_P on pO_2 has been historically used as an effective method to gain valuable insights into the ORR mechanisms. We use the EIS spectra of Fig. 4 measured at 600°C and different pO_2 as an example to illustrate the pO_2-effect on R_P. As is shown in the Nyquist plot, Fig. 4a, $R_{p(LF)}$ dominates the total R_P, particularly for the pristine sample, and increases with lowering Po_2. The latter is well expected as a result of the p-type conducting behavior in LSM. The f_{max} of the MC-modified sample is shifted to higher value compared to the pristine cathode. In general, the dependences of $R_{p(LF)}$ and $R_{p(HF)}$ of the MC-modified cathode on pO_2 is weaker than those of the pristine sample. From the Bode plot, it is more evident that the addition of carbonate has resulted in an apparent shift in frequency response. For instance, the pristine cathode shows a systematic increase in -Z" and shift in frequency to lower end with decreasing pO_2, while the MC-modified cathode only shows increase in -Z", but no clear trend of frequency change with decreasing pO_2.

The logarithmic R_P obtained from the equivalent electrical circuit fitting are plotted as a function pO_2 in Fig. 5. A linear relationship is observed for all the R_p, which suggests the following relationship between R_p and pO_2:[27,33–35]

$$R_P \propto (p_{O_2})^{-m} \quad [4]$$

where m-value is an integer dependent on the type of active species involved in ORR. For example, m = 0.48 (close to 0.5) for $R_{P(HF)}$ of the pristine cathode would suggest surface diffusion of active oxygen species as a possible rate-limiting step,[34] while a reduced m = 0.16 for $R_{P(HF)}$ of the MC-modified cathode implies that the rate-limiting

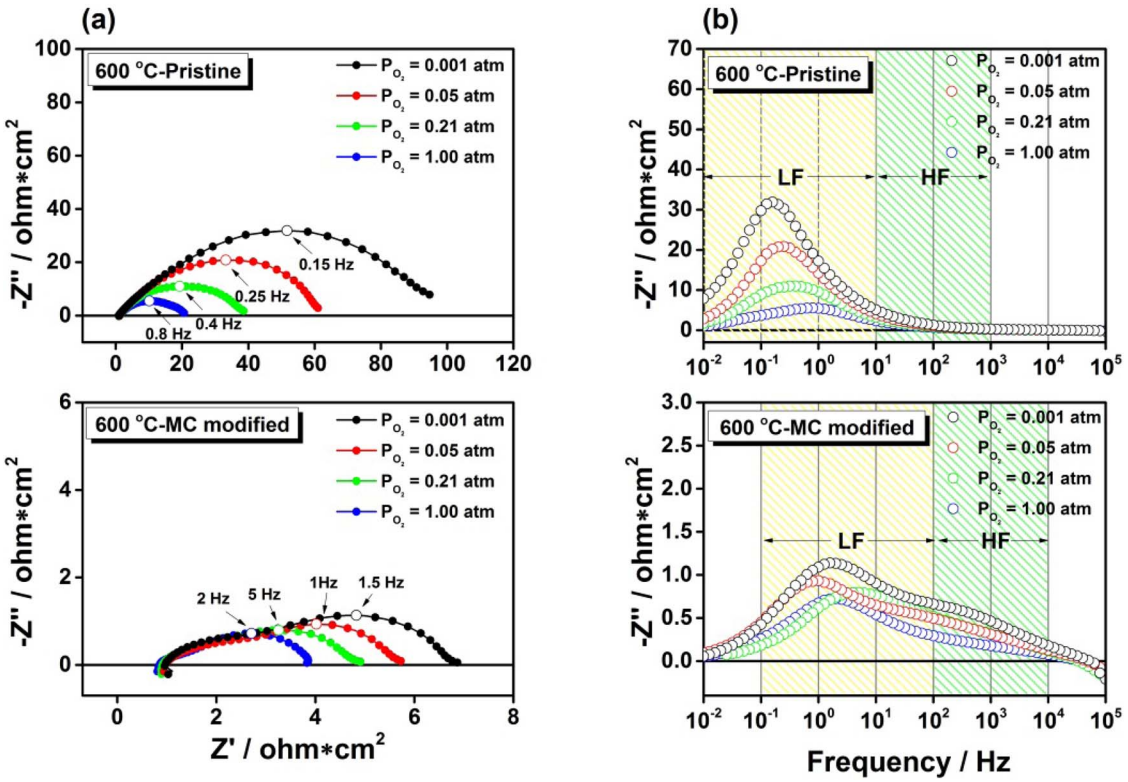

Figure 4. EIS spectra of the pristine and MC-modified cathodes measured at 600°C under different pO_2. (a) Nyquist plot, (b) Bode plot.

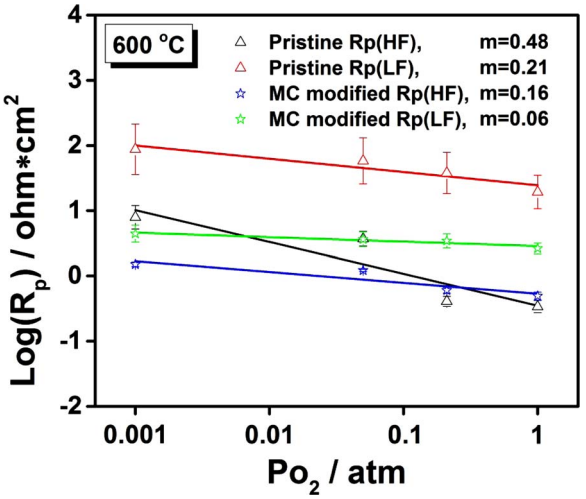

Figure 5. Dependence of $R_{p(HF)}$ and $R_{P(LF)}$ on pO_2 of the pristine and MC-modified cathodes measured at 600°C.

step has shifted to the charge-transfer like process.[33] In contrast, the $R_{P(LF)}$ shows a relatively weaker dependence on pO_2, with m = 0.21 (close to 0.25) for the pristine and 0.06 (close to zero) for the MC-modified cathodes, respectively. The former implies surface oxygen dissociative adsorption as a possible rate-limiting step,[4,5] whereas the latter signals the appearance of a new rate-limiting step, which will be further discussed below. A summary of all the reaction orders m extracted from $R_{P(HF)}$- and $R_{P(LF)}$-pO_2 dependences at different temperatures are listed in Table II.

Microstructure and fuel cell performance.— A cross-sectional view of the microstructures from the pristine and MC-modified LSGM/GDC cathode before and after EIS measurements is shown

Table II. Dependence of $R_{p(HF)}$ and $R_{p(LF)}$ on pO_2 of the pristine and MC-modified cathodes measured at different temperatures.

Temperature (°C)	m in $R_{p(HF)} \propto pO_2^{-m}$		m in $R_{p(LF)} \propto pO_2^{-m}$	
	Pristine	MC-modified	Pristine	MC-modified
650	0.32	0.14	028	0.11
600	0.48	0.16	0.21	0.06
550	0.53	0.10	0.21	0.07
500	0.47	0.08	0.22	0.08

in Fig. 6. As is clearly seen, LSM and GDC phases in the pristine cathode exhibit good neck-to-neck connections with large number three-phase boundaries (gas, LSM, GDC) for ORR to take place. The bonding between the cathode and electrolyte is also intimate, ensuring an easy ionic transfer across the interface. The microstructure shown in Fig. 6b after EIS measurement did not seem to change.

The microstructure of MC-modified cathode is very different from that of the pristine one. Fig. 6c shows it after MC incorporation but before EIS measurement. The carbonate phase is clearly shown a full coverage of the pores and the outer surfaces of LSM and GDC particles throughout the thickness of the cathode (~20 μm), even reaching out to the cathode/electrolyte interface. After EIS measurement, a rearrangement of carbonate phase within the cathode microstructure appears to have occurred, Fig. 6d, resulting in a recovery of porosity from the original "filled-up" state and formation of a thin surface layer between MC and LSM/GDC. A good wettability between MC and LSM[36] as well as GDC[37] as previously reported would seem to support the formation of the thin surface layer.

The beneficial effect of MC modification on cathode was further confirmed by the testing results of a commercial YSZ-NiO anode-supported thin-film YSZ electrolyte SOFC containing a MC-modified LSM/GDC cathode. Fig. 7 shows V-I curve and EIS spectrum of both pristine and MC-modified cells at 600°C. It is evident that MC modification has resulted in an almost two-fold power enhancement

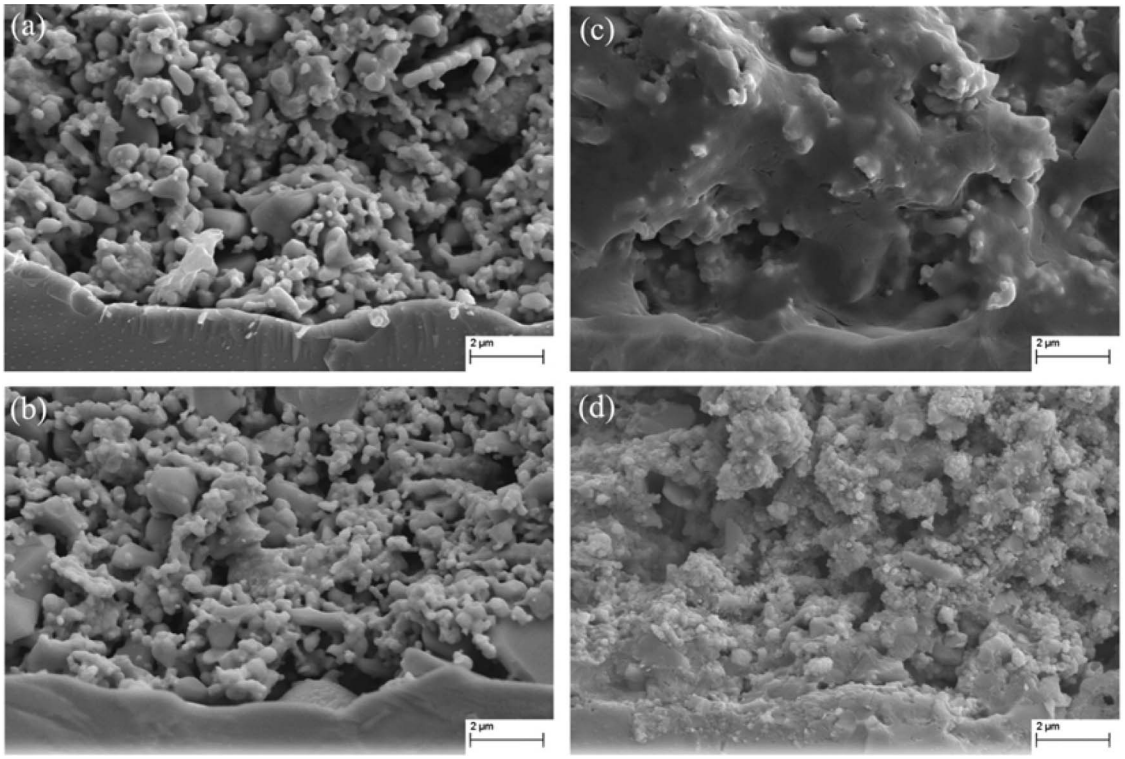

Figure 6. Cross-sectional view of LSM/GDC cathode microstructure: Pristine sample: (a) before test, (b) after test; MC-modified sample: (c) before test, (d) after test.

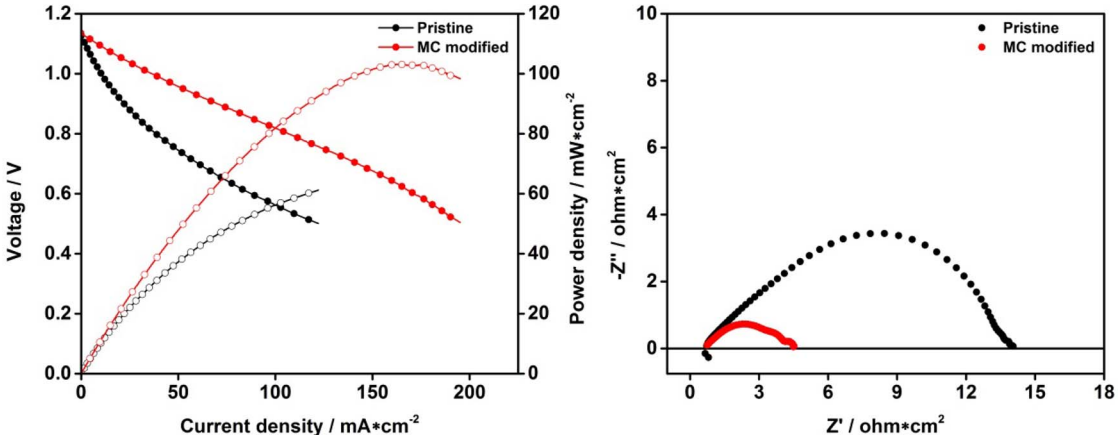

Figure 7. Electrochemical performance of a commercial cell with the pristine and MC-modified LSM/GDC cathodes measured at 600°C. (a) V-I curve; (b) EIS spectrum.

with a nearly three-fold reduction in total cell resistance. It is believed that the improved SOFC performance is attributed to the very same reason as that of the symmetrical cells, *i.e.* significant reduction in cathode polarization resistance by the presence of MC phase, even though a direct translation of R_P obtained from EIS to single cell performance is not a fair exercise due to the interference of anode and electrical current.

Discussion on mechanisms of MC-involved ORR.— Based on the results of this and other studies,[11,12] it is rather clear that a MC can appreciably lower R_P by promoting ORR activity in the temperature range of 500–650°C. Early research in MCFC has identified peroxide-ions (O_2^{2-}) and superoxide-ions (O_2^-) as the active intermediate species.[14,38–40] In the new electrochemical charge-transfer model, we further extends the active intermediate species to CO_4^{2-} and CO_5^{2-} based on the very recent results obtained from DFT calculations[11] and in-situ Raman spectroscopy.[19]

Combining this charge-transfer model and EIS results, we discuss in the following the understanding of rate-limiting steps for the MC-involved ORR. First, given the large $R_{p(LF)}$ of the pristine cathode and $m \approx 0.25$, the low-frequency response for the pristine LSM/GDC cathode is thought to be the rate-limiting step resulting from oxygen dissociative adsorption.[5,41] As a consequence, the low concentration of adsorbed oxygen species, $[O_{ad}]$, limits the surface diffusion that leads to $m \approx 0.5$ for the high-frequency response below 600°C.[34] Low sticky coefficient of O_2 molecules onto a solid surface is the likely cause for the observed sluggish dissociative chemisorption.

In contrast, MC can provide a "soft" surface for O_2 molecules to stick on, and allow O_2 to further chemically dissolve into MC as species CO_5^{2-}. A restructuring of CO_5^{2-} within CO_3^{2-} results in the formation of CO_4^{2-}, which is perceived mobile via a cooperative "cogwheel" mechanism toward cathode surface where it is further reduced by e^- from LSM into CO_3^{2-} and O^{2-}. Obviously, the rate of CO_4^{2-} generation and the ionic supply of CO_3^{2-} should be properly balanced, since the Li-Na-K ternary carbonate system possesses a relatively low ionic conductivity of 1.25 $S \cdot cm^{-1}$ at 600°C.[42] The occurrence of an optimal MC loading reflects the best balance between the two.

Based on the dependence of R_P on pO_2, the elementary steps for MC-involved ORR are hypothesized as follows:

$$CO_3^{2-}{}_{(MC)} + O_{2(air)} \rightarrow CO_5^{2-}{}_{(MC)} \quad m = 1 \qquad [5]$$

$$CO_5^{2-}{}_{(MC)} + CO_3^{2-}{}_{(MC)} \rightarrow 2CO_4^{2-}{}_{(MC)} \quad m = 0 \qquad [6]$$

$$CO_4^{2-}{}_{(MC)} + e^-_{(LSM)} \rightarrow CO_3^{2-}{}_{(MC)} + O^-{}_{(MC)} \quad m = 0.375 \qquad [7]$$

$$O^-_{(MC)} + e^-_{(LSM)} \rightarrow O^{2-}_{(LSM-GDC-MC)} \quad m = 0.125 \qquad [8]$$

$$O^{2-}_{(LSM-GDC-MC)} \rightarrow O^{2-}_{(LSGM)} \quad m = 0 \qquad [9]$$

The theoretical reaction orders m with respect to pO_2 for each step are also shown with each elementary reaction.[43] Compared to these values, the approximate $R_{p(HF)} \propto P_{O_2}^{-0.125}$ dependence infers charge-transfer process (8) involving $O^-{}_{(MC)}$ and $O^{2-}{}_{(LSM-GDC-MC)}$ as the rate-limiting step. However, the weak $R_{p(LF)} \propto P_{O_2}^{-0.06\sim-0.11}$ dependence appears to deviate from the $P_{O_2}^{-0.5}$ dependence as expected for chemisorption of oxygen molecules. The smaller m-value suggests the generation of CO_4^{2-} from CO_5^{2-} andCO_3^{2-} (Step (6)) as a possible rate-limiting step. One reason for this assumption might be relevant to the low local concentrations of CO_3^{2-} and CO_5^{2-} at the narrow gas/carbonate interface. These reactant ions are interrelated as CO_5^{2-} is produced at the cost of CO_3^{2-}. Another possible reason is the endothermic nature to break the oxygen-bond in CO_5^{2-} through reaction 3.[11,13] Overall, the significantly increased number of oxygen-carrier species by the presence of MC, which is reflected in the increased exponential factor A in the Arrhenius plot of $1/R_{p(LF)}$, substantially boost the rate of oxygen dissociative adsorption reflected by $R_{p(LF)}$ of the pristine cathode, resulting in a significant promotion of the ORR activity in a MC-modified LSM/GDC cathode.

Conclusions

The effect of MC on the ORR activity of a composite SOFC cathode LSM/GDC has been systematically studied in the temperature range of 550–650°C and pO_2 span of $10^{-3} \sim 1$ atm with EIS method. The EIS spectra measured can be reasonably modeled by two R_P//CPE components across the entire frequency domain. Comparison of R_P quantified from the equivalent electrical circuit model for the pristine and MC-modified LSM/GDC cathode indicates as much as a factor of ten reductions in R_P, primarily from the low-frequency part of R_P, by the presence of an optimal amount of MC phase. The Arrhenius plots of R_P reveal that the reduction is principally originated from the pre-exponential term, not the activation energy, inferring that the probability of a reaction or the rate of ORR has been enhanced by the liquid carbonate phase. The dependence of $R_{P(LF)}$ on pO_2 further suggests the surface oxygen dissociative adsorption as a rate-limiting step for the pristine LSM/GDC and the formation of intermediate surface species CO_4^{2-} as a rate-limiting step for the MC-modified cathode.

Acknowledgments

We thank NSF (CBET-1340269, CBET-124706) and the U. S. Army Research Laboratory and the U. S. Army Research Office (W911NF-10-R-006) for financial support.

References

1. N. Q. Minh, *J. Am. Ceram. Soc.*, **76**, 563 (1993).
2. B. C. H. Steele, *Solid State Ionics*, **86-8**, 1223 (1996).
3. S. B. Adler, *Chem Rev*, **104**, 4791 (2004).
4. E. P. Murray, T. Tsai, and S. A. Barnett, *Solid State Ionics*, **110**, 235 (1998).
5. E. P. Murray and S. A. Barnett, *Solid State Ionics*, **143**, 265 (2001).
6. M. Juhl, S. Primdahl, C. Manon, and M. Mogensen, *J. Power Sources*, **61**, 173 (1996).
7. Y. H. Gong, W. J. Ji, B. Xie, and H. Q. Wang, *Solid State Ionics*, **192**, 505 (2011).
8. V. A. C. Haanappel, J. Mertens, D. Rutenbeck, C. Tropartz, W. Herzhof, D. Sebold, and F. Tietz, *J. Power Sources*, **141**, 216 (2005).
9. T. Z. Sholklapper, H. Kurokawa, C. P. Jacobson, S. J. Visco, and L. C. De Jonghe, *Nano Lett*, **7**, 2136 (2007).
10. Z. Y. Jiang, L. Zhang, K. Feng, and C. R. Xia, *J. Power Sources*, **185**, 40 (2008).
11. C. Y. Qin and A. Gladney, *Comput. Theor. Chem.*, **999**, 179 (2012).
12. Y. Gong, X. Li, L. Zhang, W. Tharp, C. Qin, and K. Huang, *J. Electrochem. Soc.*, **160**, F958 (2013).
13. A. J. Appleby and S. B. Nicholson, *J. Electroanal. Chem.*, **112**, 71 (1980).
14. C. Y. Yuh and J. R. Selman, *J. Electrochem. Soc.*, **138**, 3642 (1991).
15. X. Li, N. S. Xu, L. L. Zhang, and K. Huang, *Electrochem. Commun.*, **13**, 694 (2011).
16. M. Jansen, *Angew. Chem.-Int. Edit. Engl.*, **30**, 1547 (1991).
17. S. Shin, Y. Tezuka, A. Sugawara, and M. Ishigame, *Phys. Rev. B*, **44**, 11724 (1991).
18. N. Bagdassarov, H. C. Freiheit, and A. Putnis, *Solid State Ionics*, **143**, 285 (2001).
19. L. J. Chen, C. J. Lin, J. Zuo, L. C. Song, and C. M. Huang, *J. Phys. Chem. B.*, **108**, 7553 (2004).
20. C. C. Kan, H. H. Kan, F. M. Van Assche, E. N. Armstrong, and E. D. Wachsman, *J. Electrochem. Soc.*, **155**, B985 (2008).
21. Y. M. Choi, M. C. Lin, and M. L. Liu, *J. Power Sources*, **195**, 1441 (2010).
22. Y. H. Gong, C. Y. Qin, and K. Huang, *ECS Electrochem. Lett.*, **2**, F4 (2013).
23. K. Q. Huang, R. S. Tichy, and J. B. Goodenough, *J. Am. Ceram. Soc.*, **81**, 2565 (1998).
24. C. R. Xia, W. Rauch, W. Wellborn, and M. L. Liu, *Electrochem. Solid State Lett.*, **5**, A217 (2002).
25. F. H. van Heuveln, H. J. M. Bouwmeester, and F. P. F. van Berkel, *J. Electrochem. Soc.*, **144**, 126 (1997).
26. M. J. Jorgensen and M. Mogensen, *J. Electrochem. Soc.*, **148**, A433 (2001).
27. F. H. van Heuveln and H. J. M. Bouwmeester, *J. Electrochem. Soc.*, **144**, 134 (1997).
28. C. H. Hsu and F. Mansfeld, *Corrosion*, **57**, 747 (2001).
29. S. Bebelis, N. Kotsionopoulos, A. Mai, D. Rutenbeck, and F. Tietz, *Solid State Ionics*, **177**, 1843 (2006).
30. J. N. Soderberg, L. Sun, P. Sarkar, and V. I. Birss, *J. Electrochem. Soc.*, **156**, B721 (2009).
31. N. T. Hart, N. P. Brandon, M. J. Day, and J. E. Shemilt, *J Mater Sci*, **36**, 1077 (2001).
32. S. W. Zha, Y. L. Zhang, and M. L. Liu, *Solid State Ionics*, **176**, 25 (2005).
33. J. D. Kim, G. D. Kim, J. W. Moon, Y. I. Park, W. H. Lee, K. Kobayashi, M. Nagai, and C. E. Kim, *Solid State Ionics*, **143**, 379 (2001).
34. Y. Takeda, R. Kanno, M. Noda, Y. Tomida, and O. Yamamoto, *J. Electrochem. Soc.*, **134**, 2656 (1987).
35. M. J. Escudero, A. Aguadero, J. A. Alonso, and L. Daza, *J. Electroanal. Chem.*, **611**, 107 (2007).
36. B. Huang, S. R. Wang, Q. C. Yu, Y. Liu, and K. A. Hu, *J. Appl. Electrochem.*, **35**, 1145 (2005).
37. B. Zhu, *J. Power Sources*, **114**, 1 (2003).
38. P. L. Spedding and R. Mills, *J. Electrochem. Soc.*, **112**, 594 (1965).
39. A. J. Appleby and C. Vandrunen, *J. Electrochem. Soc.*, **127**, 1655 (1980).
40. R. W. Reeve and A. C. C. Tseung, *J. Electroanal. Chem.*, **403**, 85 (1996).
41. J. VanHerle, A. J. McEvoy, and K. R. Thampi, *Electrochim. Acta*, **41**, 1447 (1996).
42. T. Kojima, Y. Miyazaki, K. Nomura, and K. Tanimoto, *J. Electrochem. Soc.*, **155**, F150 (2008).
43. A. J. Appleby and S. B. Nicholson, *J. Electroanal. Chem.*, **83**, 309 (1977).